crystals

MDPI

Article

Growth and Scintillation Properties of Directionally Solidified Ce:$LaBr_3$/$AEBr_2$ (AE = Mg, Ca, Sr, Ba) Eutectic System

Kyoung Jin Kim [1,2,*], Yuki Furuya [3], Kei Kamada [1,2], Rikito Murakami [2,3], Vladimir V. Kochurikhin [2], Masao Yoshino [3], Hiroyuki Chiba [3], Shunsuke Kurosawa [1], Akihiro Yamaji [3], Yasuhiro Shoji [2,3], Satoshi Toyoda [1], Hiroki Sato [1], Yuui Yokota [3], Yuji Ohashi [1] and Akira Yoshikawa [1,2,3]

1 New Industry Creation Hatchery Center (NICHe), Tohoku University, 6-6-10 Aoba, Aramaki, Aoba-ku, Sendai 980-8579, Japan; kamada@imr.tohoku.ac.jp (K.K.); kurosawa@imr.tohoku.ac.jp (S.K.); toyoda@imr.tohoku.ac.jp (S.T.); h.sato@imr.tohoku.ac.jp (H.S.); ohashi@imr.tohoku.ac.jp (Y.O.); yoshikawa@imr.tohoku.ac.jp (A.Y.)

2 C&A Corporation, 1-16-23 Ichibancho, Aoba-ku, Sendai 980-0811, Japan; r_murakami@imr.tohoku.ac.jp (R.M.); kochurikhin@c-and-a.jp (V.V.K.); y_shoji@imr.tohoku.ac.jp (Y.S.)

3 Institute for Material Research (IMR), Tohoku University, 2-1-1 Katahira, Aoba-ku, Sendai 980-8577, Japan; fyuki@imr.tohoku.ac.jp (Y.F.); yoshino.masao@imr.tohoku.ac.jp (M.Y.); chiba-hiro@imr.tohoku.ac.jp (H.C.); yamaji-a@imr.tohoku.ac.jp (A.Y.); yokota@imr.tohoku.ac.jp (Y.Y.)

* Correspondence: kjkim72@imr.tohoku.ac.jp; Tel.: +81-22-215-2214; Fax: +81-22-215-2215

Received: 5 June 2020; Accepted: 2 July 2020; Published: 6 July 2020

Abstract: Ce-doped $LaBr_3$/$AEBr_2$ (AE = Mg, Ca, Sr, Ba) eutectics were grown using the Bridgman–Stockbarger (BS) method in quartz ampoules. The eutectics (AE = Mg and Ca) showed optical transparency like optical fiber bundles. A grown Ce-doped $LaBr_3$/$MgBr_2$ eutectic shows a 355 nm emission ascribed to Ce^{3+} 4f-5d transition under X-ray excitation. The smaller the ionic size of AE, the higher the light yield of the sample was. The light yield of Ce:$LaBr_3$/$MgBr_2$ was 34,300 photon/MeV, which is higher than Ce:LYSO standard. Scintillation decay time under 662 keV gamma-ray excitation was 18.8 ns.

Keywords: directional solidification; growth from melt; halides; scintillators

1. Introduction

Scintillators coupled with photodetectors are widely used in radiation imaging applications such as medical imaging, security, high-energy physics, astrophysics, oil well logging, etc. In order to meet the needs of these applications, a deeper knowledge of crystal physics and all the mechanisms involved in their scintillating behavior is important [1]. In conventional high-resolution radiation imaging systems employing inorganic scintillators, scintillation light must be guided to photo-sensors efficiently without lateral light diffusion [2]. In X-ray imaging applications, radiation imaging sensors are composed of photodetector arrays and an indirect flat panel detector (FPD) coupled with a scintillator plate such as Tl:CsI [3,4] or Tb:Gd_2O_2S (GOS) [5,6]. Improvement in spatial resolution is required in this application. However, columnar grown Tl:CsI reduces the spatial resolution because of light scattering in micrometer size Tl:CsI fiber crystals [3]. Light diffusion through scintillator materials on photodetector degrades the resolution of radiation imaging sensors and limits sensitivity. Recently, pixelated photodetector arrays have been improved in order to achieve a micrometer scale spatial resolution. However, the pixel size of scintillator arrays and light diffusion limit the spatial resolution. Moreover, X-ray energy-resolved counting systems using silicon photomultipliers (SiPM)

and scintillators are being developed now. In such systems, inorganic scintillators with fast and good energy resolution are required [7].

Currently, submicron-diameter phase-separated scintillator fibers (PSSFs) have been reported and they have both characteristics of optical fiber and a radiation-to-light conversion. PSSFs were realized by a directionally solidified eutectic (DSE) growth in previous research [8–12]. In PSSFs, the emitted scintillation is confined and transported along the eutectic structure by a total reflection mode, so that light diffusion can be reduced and high-resolution imaging can be achieved. Research on PSSFs such GAP/α-Al_2O_3 [13,14], $SrHfO_3/Al_2O_3$ [15], $Gd_2Si_2O_7/SiO_2$ [16], and $LiF/CaF_2/LiBaF_3$ [17] has been previously reported by our group.

In order to find a good combination of eutectic structure with PSSFs, the choice of scintillator materials is important. The Ce:$LaBr_3$ scintillator has attracted attention due to its high light yield of over 74,000 photon/MeV and fast decay time of around 20 ns, with enough density of 5.1 g/cm^3 for low energy X-ray detection even though it is hygroscopic [18,19]. In this research, exploration of PSSFs by directional crystal growth method is reported. Ce-doped $LaBr_3/AEBr_2$ (AE = Mg, Ca, Sr, Ba) eutectics were investigated. Here, we designed the matrix $AEBr_2$ phase and scintillation $LaBr_3$ fibers at the eutectic point of $LaBr_3/AEBr_2$ (See Figure 1). Crystal growth was performed using the Bridgman–Stockbarger (BS) method at the eutectic point. Investigations of the crystal structure and eutectic phase were performed. Luminescence and scintillation properties were also evaluated.

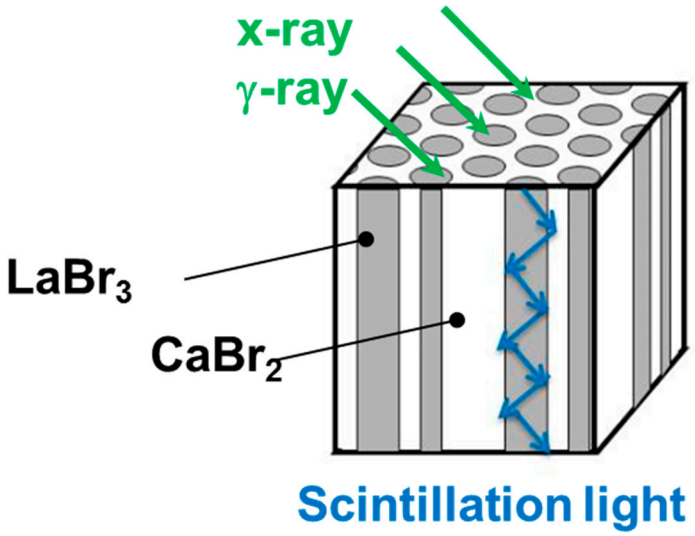

Figure 1. Schematic diagram of generation of scintillation light in the eutectic.

2. Experimental Procedure

2.1. Crystal Growth

The starting materials were prepared from high-purity halide powders of $CeBr_3$, $LaBr_3$, and $AEBr_2$ (3N, produced by APL, AE = Mg, Ca, Sr, Ba) according to the molar ratio of $AEBr_2$:$LaBr_3$:$CeBr_3$ = 75:24.75:0.25. Crystal growth was carried out via the BS method in a quartz ampoule with an inner diameter of 4 mm for AE = Ca and an inner diameter of 8 mm for AE = Mg, Sr, and Ba. Details of crystal growth by the BS method are given in Figure 2. In the unidirectional solidification processes, $LaBr_3$ and $AEBr_2$ phases deposit from the melt on their own formed solid phases. The mixed powders were put into a quartz ampoule inside the glovebox in 9N Ar atmosphere. The quartz ampoule was then taken from the glovebox and baked in high vacuum (~10^{-4} Pa) at 200 °C using 9N purity Ar and $SiCl_4$ gas to remove water and oxygen. We carefully evacuated and sealed off the ampoule with an oxyhydrogen burner. After sealed cutting, each ampoule was set into a furnace and heated by a carbon heater with the radio-frequency induction coil. The pull down speed for crystal growth was 0.5 mm/min. After the crystal growth was finished, the furnace was gradually cooled down to

room temperature. Plates with a thickness of 1 mm were cut from the grown samples. They were double side polished for back-scattered electron image (BEI) evaluation, luminescence, and scintillation property measurements.

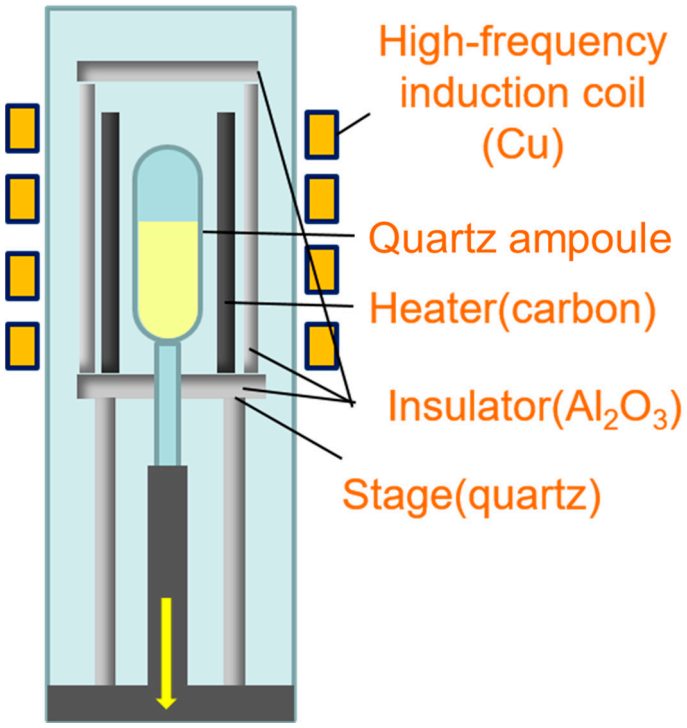

Figure 2. The schematic drawing of crystal growth via the Bridgman–Stockbarger (BS) method. The ampoules used have outer and inner diameters of 10 and 8 mm, respectively.

2.2. Structural Evaluation of Eutectic Composites

From the grown crystals, round and rectangular samples with a thickness of 1 mm were obtained and the cut surface was optically polished. The eutectic phase structure in the grown crystals was observed by BEI (S-3400N SEM, Hitachi, Tokyo, Japan). The eutectic structures in transverse and vertical cross-sections were observed. The obtained phases in the eutectics were investigated by powder X-ray diffraction (XRD) in the 2θ range from 20 to 60° using X-ray diffractometer (RINT-2000, Rigaku, Akishima, Japan). The X-ray source was CuKα with an accelerating voltage of 40 kV and tube current of 40 mA.

2.3. Measurements of Luminescence and Scintillation Properties

The radioluminescence spectra under X-ray irradiation (40 mV, 30 mA) were recorded with a spectrometer (SR-163, Andor Technology, Belfast, UK), equipped with a spectroscopy CCD detector (DU920P, Andor Technology, Belfast, UK). The light output was measured using a photomultiplier tube (PMT) (R7600U-200, Hamamatsu Photonics, Hamamatsu, Japan) with an ultra bialkali photocathode. The samples were coupled with the PMT using silicone grease (OKEN, 6262A) and covered using Teflon-tape. To determine the light yield, the energy spectra were collected under 662 keV γ-ray excitation (^{137}Cs source) using a PMT. The signal was fed into a shaping amplifier (572A, ORTEC, Oak Ridge, TN, USA), digitized by a multichannel analyzer (MCA) (926, ORTEC, Oak Ridge, TN, USA), and finally sent to a personal computer. The shaping time was set to 2 μs. The bias for the PMT was supplied by ahigh-voltage power supply (ORTEC, Oak Ridge, TN, USA). The same setting as the PMT and digital oscilloscope (TDS 5032B, Tektronix, Beaverton, OR, USA) was used to measure the scintillation decay time.

3. Results and Discussion

3.1. DSE System of $LaBr_3$/$AEBr_2$ Eutectic

White rod-shaped samples were obtained via the BS method. Grown samples and 1 mm thick plates after polishing are shown in Figure 3. For AE = Mg or Ca, the samples showed optical transparency like optical fiber bundles. Therefore, the background line was visible on the surface through the transparent rods grown in the material, while the samples were not transparent through the radial direction. For AE = Sr or Ba, the samples showed optical transparency. Therefore, the background line was visible on the surface through the grown crystal, and the samples were semitransparent through the radial direction.

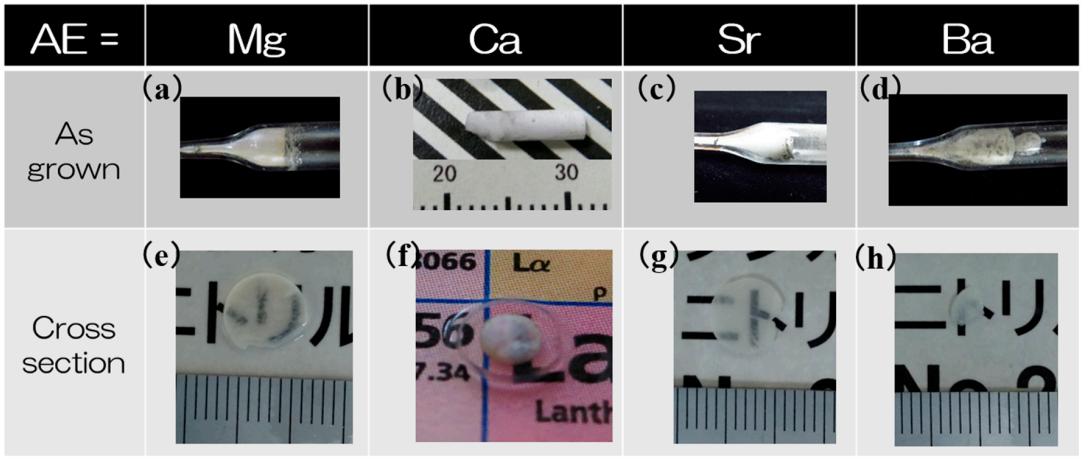

Figure 3. Photographs of the (**a**–**d**) as grown Ce:$LaBr_3$/$AEBr_2$ samples (AE = Mg, Ca, Sr, Ba) and (**e**–**h**) cross-section polished samples (AE = Mg, Ca, Sr, Ba).

The grown samples were crushed into powder in a glovebox in 9N Ar atmosphere and packaged into an atmosphere-controllable sample case. Powder XRD measurements were performed using the sample case. The results of powder XRD of the grown samples were shown in Figure 4. For AE = Mg or Ca, the grown eutectics showed two main phases of $LaBr_3$ (crystal system: hexagonal, space group: P63/m) and $MgBr_2$ (crystal system: trigonal, space group: P-3m1), or $CaBr_2$ (crystal system: trigonal, space group: Pnnm). For AE = Sr or Ba, the grown samples showed only a single phase. For AE = Sr, the main phase was $SrBr_2$ (Crystal System: tetragonal, Space Group: P4/n z). Almost all peaks were $SrBr_2$ peaks except for a peak around 29 degrees, which was assumed to be a trace of hydroxyl bromide coming from a hygroscopic characteristic of $LaBr_3$ and $SrBr_2$ or $BaBr_2$ during the crushing. For AE = Ba, main phase had an unknown composition. That main phase was thought to be a compound of $LaBr_3$ and $BaBr_2$. The powder XRD pattern of this compound has not been identified with the existing powder diffraction file (PDF) database. Therefore, additional research is needed for detailed phase identification. The BEI of the grown samples in vertical and transverse cross-sections are shown in Figure 5. For AE = Mg or Ca, the grown eutectic structure showed a mixture of the rod and plate shapes of $LaBr_3$ phase surrounded by a $MgBr_2$ or $CaBr_2$ matrix. This mixed structure of $LaBr_3$ was aligned with a length of around 150–200 μm. Previously, some groups have investigated transformation between the rod-like shape and lamellar shape in eutectic structure [20–23]. They concluded that the transformation of the eutectic depended on the volume ratio of components and the relative interface energy. The rod-like shape can be obtained at a volume ratio of around 30–40% [24]. Volume ratio of $LaBr_3$:$AEBr_2$ in this system is about 25:75, and the $LaBr_3$/$CaBr_2$ or $LaBr_3$/$MgBr_2$ eutectic can take a rod-like shape structure by optimizing temperature gradient along the growth direction and growth rate [25]. Scintillation light from $LaBr_3$ phase shows around 57° of total reflection at the interface. In this report, though a well-aligned rod-like shape structure could not be obtained, optical transparency like

optical fiber bundles was observed in the eutectic. For AE = Sr or Ba, the grown crystal did not show a $LaBr_3/AEBr_2$ eutectic structure and showed only one phase.

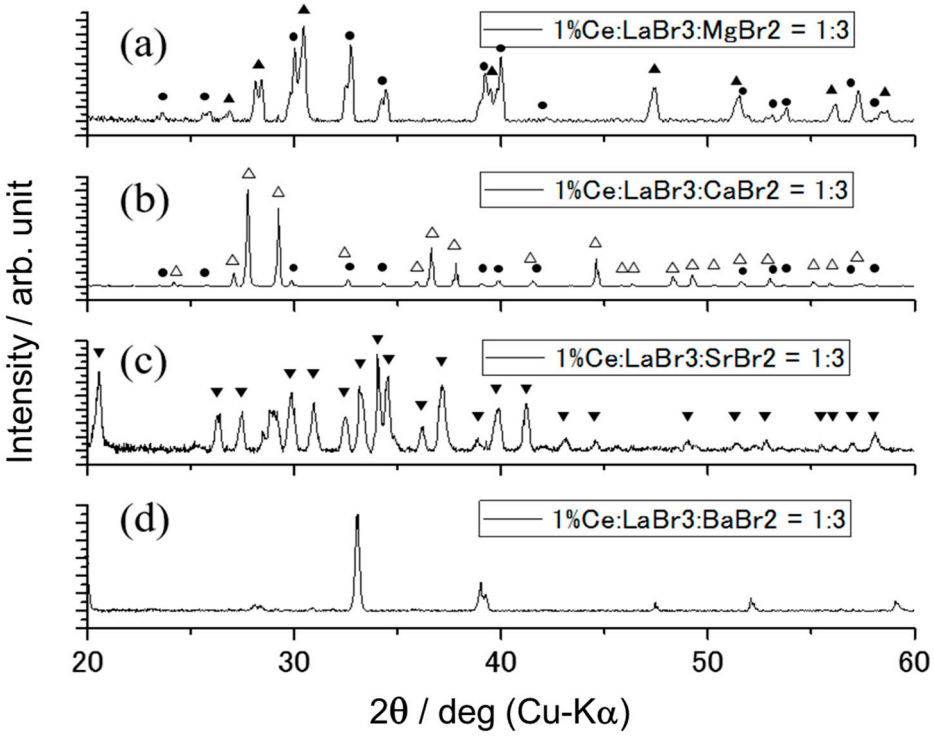

Figure 4. X-ray diffraction patterns of grown samples. (**a**) AE = Mg, (**b**) AE = Ca, (**c**) AE = Sr, (**d**) AE = Ba. (●): peaks of $LaBr_3$ (hexagonal, P63/m), (▲): peaks of $MgBr_2$ (trigonal, P-3mL), (△): peaks of $CaBr_2$ (trigonal, Pnnm), (▼): peaks of $SrBr_2$ (tetragonal, P4/n z).

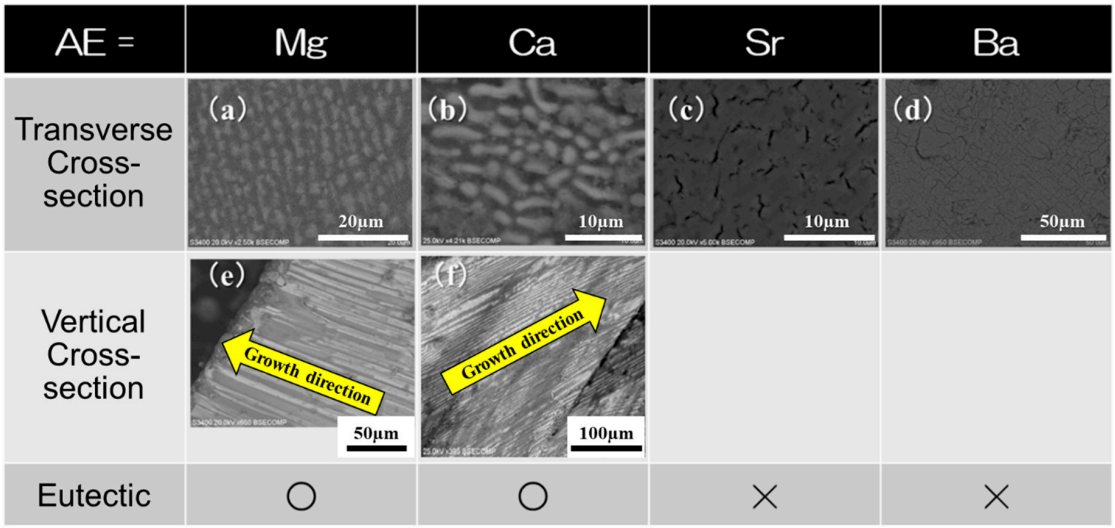

Figure 5. Back-scattered electron image (BEI) of the polished $LaBr_3/AEBr_2$ crystals, (**a**–**d**) transverse cross-section for AE = Mg, Ca, Sr, Ba and (**e**,**f**) vertical cross-section along growth direction for AE = Mg and Ca.

3.2. Luminescence and Scintillation Properties

Radioluminescence spectra of the grown Ce-doped $LaBr_3/AEBr_2$ (AE = Mg, Ca, Sr, Ba) eutectic measured under X-ray irradiation are shown in Figure 6. All samples show the typical double-band Ce^{3+} 5d-4f emission with maxima at around 355 and 385 nm according to the transitions into the $^2F_{5/2}$ and $^2F_{7/2}$ states, respectively. These results are in good agreement with previous reports [18,19].

Emission peaks were slightly shifted to the short wavelength region except for AE = Ba (AE = Mg:350 nm, 383 nm, AE = Ca:354 nm, 384 nm, AE = Sr:353 nm, 379 nm). For AE = Ba, emission peaks were slightly shifted to the long wavelength region (362 nm, 389 nm), due to its difference in crystal structure.

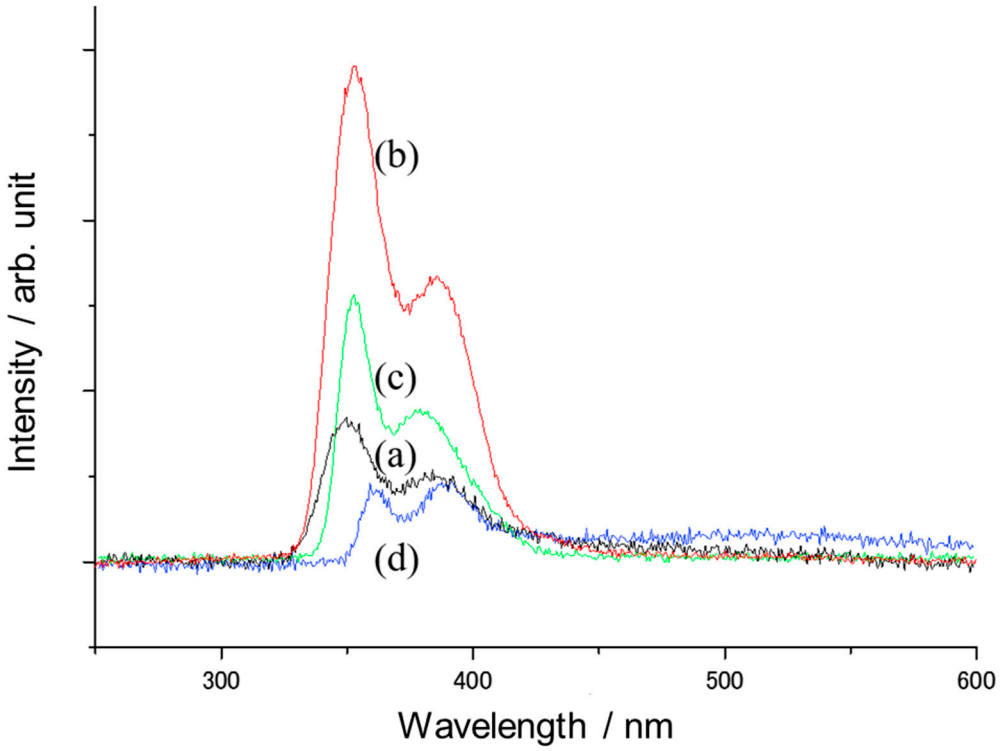

Figure 6. Radioluminescence spectra of the grown samples measured under X-ray irradiation. (**a**) AE = Mg, (**b**) AE = Ca, (**c**) AE = Sr, (**d**) AE = Ba.

The pulse-height spectra of the eutectic sample excited by 662 keV gamma-rays of ^{137}Cs at room temperature and measured using the PMT are shown in Figure 7. Light outputs of the samples were around 1.07, 0.53, 0.43, and 0.18 of the Ce:LYSO standard with 32,000 photon/MeV [26,27] for AE = Mg, Ca, Sr, Ba, respectively. Therefore, light outputs of samples were around 34,300, ~17,000, ~14,000, and ~6000 photon/MeV for AE = Mg, Ca, Sr, and Ba, respectively. The scintillation decay curves of the samples excited by 662 keV gamma-rays are shown in Figure 8. In the case of $LaBr_3/BaBr_2$, enough intensity of the decay curve signal was not detected due to its weak light output. Table 1 shows the survey of light yield and scintillation decay time values for all samples. For all samples, decay times were comparable to Ce:$LaBr_3$ single crystal and had slower components except for $LaBr_3/MgBr_2$. This matches with past results [18,19]. The smaller the ionic size of AE, the faster the components decay.

Table 1. Light output and decay components of the Ce:$LaBr_3$/$AEBr_2$ samples (AE = Mg, Ca, Sr, Ba).

	Peak Channel	Light Yield (Photon/MeV)	Scintillation Decay Time	
			1st Component (ns)	2nd Component (ns)
$LaBr_3/MgBr_2$	1512	34,300	18.8 (100%)	-
$LaBr_3/CaBr_2$	750	~17,000	22.4 (60%)	185 (40%)
$LaBr_3/SrBr_2$	620	~14,000	38.6 (44%)	299.8 (56%)
$LaBr_3/BaBr_2$	250	~6000	N.D.	N.D.

N.D.: Not detected.

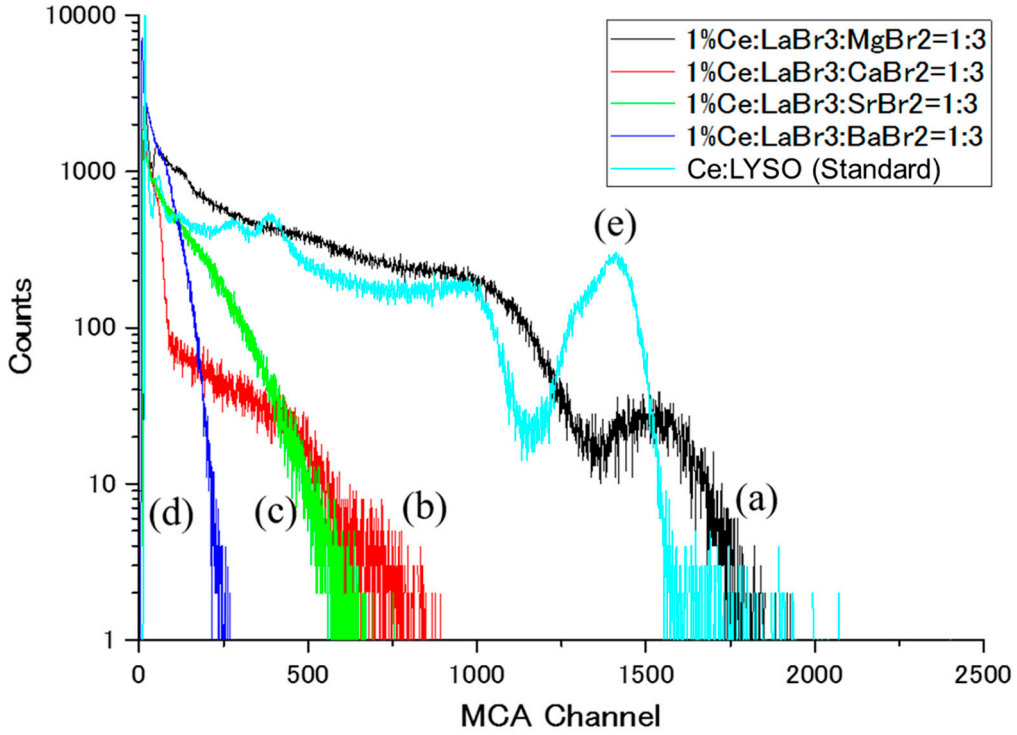

Figure 7. Energy spectra of the grown samples and Ce:LYSO standard. Excitation by ^{137}Cs radioisotope (662 keV). (**a**) AE = Mg, (**b**) AE = Ca, (**c**) AE = Sr, (**d**) AE = Ba, (**e**) Ce:LYSO standard.

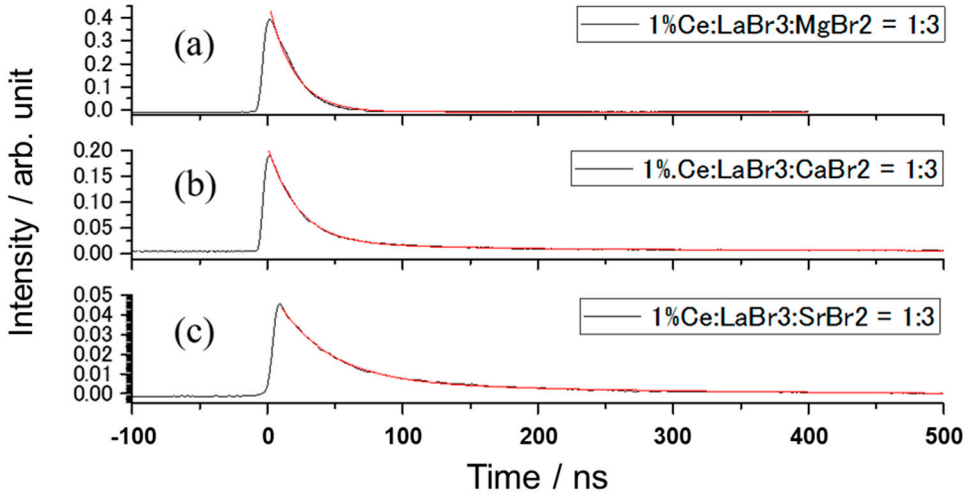

Figure 8. Scintillation decay curves of the grown samples. Excitation by ^{137}Cs radioisotope (662 keV). (**a**) AE = Mg, (**b**) AE = Ca, (**c**) AE = Sr.

4. Conclusions

Ce-doped $LaBr_3/AEBr_2$ (AE = Mg, Ca, Sr, Ba) eutectics were grown via the BS method in a quartz ampoule. For AE = Mg, Ca grown samples showed a $LaBr_3/AEBr_2$ eutectic structure. They showed optical transparency only for the growth direction through transparent rods grown in the material, while they were not transparent through the radial direction. They showed a mixture of rod and plate shapes. This mixed structure was aligned with a length of around 150–200 μm. For AE = Sr, Ba grown samples did not show a $LaBr_3/AEBr_2$ eutectic structure and showed a single phase. The Ce:$LaBr_3/AEBr_2$ samples showed a 355 nm emission ascribed to Ce^{3+} 4f-5d transition under X-ray excitation. Light outputs of samples were around 34,300, ~17,000, ~14,000, and ~6,000 photon/MeV for AE = Mg, Ca, Sr, and Ba, respectively. Scintillation decay times under 662 keV gamma-rays

were 18.8 ns (100%) for $LaBr_3/MgBr_2$, 22.4 ns (60%) and 185 ns (40%) for $LaBr_3/CaBr_2$, 38.6 ns (44%), and 299.8 ns (56%) for $LaBr_3/SrBr_2$. The smaller the ionic size of AE, the faster the components' decay. We demonstrated the possibility of a hygroscopic halide eutectic scintillator with a fast scintillation response. The light output of the Ce:$LaBr_3/MgBr_2$ eutectic was higher than Ce:LYSO standard and can be increased by getting well-aligned rod-shaped eutectic structures and improving optical transparency. If large size crystal growth and material processes for imaging application are established, $LaBr_3$-based fast eutectic scintillators can be used for radiation imaging applications such as pulse counting X-ray imaging, which requires both fast timing and high-resolution performance.

Author Contributions: Conceptualization, K.K.; Data curation, K.K. and K.J.K.; Formal analysis, K.K. and M.Y.; Funding acquisition, K.K. and K.J.K.; Investigation, Y.F., H.C. and R.M.; Methodology, K.J.K. and S.K.; Project administration, A.Y. (Akira Yoshikawa); Supervision, A.Y. (Akira Yoshikawa); Validation, A.Y. (Akihiro Yamaji), Y.S., S.T., H.S., Y.Y. and Y.O.; Writing—original draft, K.K. and K.J.K.; Writing—review & editing, K.J.K. and V.V.K. All authors have read and agreed to the published version of the manuscript.

Funding: This work was partially supported by (i) Japan Society for the Promotion of Science (JSPS) Grants-in-Aid for Scientific Research (KAKENHI) Project ID 19164606, 19164252, 19132801, 17920611 and 18057417, (ii) Projects to support the advancement of strategic core technologies, Czech Science foundation No. 15-18300Y, and MEYS No. SOLID21 CZ.02.1.01/0.0/0.0/16_019/0000760 projects, (iii) Crystal Clear Collaboration in CERN.

Conflicts of Interest: The authors declare no conflict of interest.

References

1. Rinaldi, D.; Montalto, L. Scintillator crystals: Structure, characterization and models for better performances. *Crystals* **2020**, *10*, 96. [CrossRef]
2. Tyrrell, G.C. Phosphors and scintillators in radiation imaging detectors. *Nucl. Instrum. Methods Phys. Res. Sect. A* **2005**, *546*, 180–187. [CrossRef]
3. Nagarkar, V.V.; Gaysinskiy, V.; Shestakova, I.; Singh, B.; Teo, K.; Sun, M.; Barber, W.C.; Hasegawa, B. Near simultaneous combined SPECT/CT imaging using an EMCCD. *IEEE Nucl. Sci. Symp. Conf. Rec.* **2005**, *4*, 2607–2610.
4. Michail, C.; Valais, I.; Seferis, I.; Kalyvas, N.; Fountos, G.; Kandarakis, I. Experimental measurement of a high resolution CMOS detector coupled to CsI scintillators under X-ray radiation. *Radiat. Meas.* **2015**, *74*, 39–46. [CrossRef]
5. Blasse, G.; Grabmaier, B.C. *Luminescent Materials*; Springer: Berlin/Heidelberg, Germany, 1994.
6. Howansky, A.; Lubinsky, A.R.; Suzuki, K.; Ghose, S.; Zhao, W. An apparatus and method for directly measuring the depth-dependent gain and spatial resolution of turbid scintillators. *Med. Phys.* **2018**, *45*, 4927–4941. [CrossRef]
7. Philippov, D.; Popova, E.; Vinogradov, S.; Stifutkin, A.; Pleshko, A.; Klemin, S.; Ilyin, A.; Belyaev, V.; Besson, D.; Vandychev, M. Development of SiPM-based X-ray counting scanner for human inspection. *IEEE Trans. Nucl. Sci.* **2018**, *65*, 2013–2020. [CrossRef]
8. Llorca, J.; Orera, V.M. Directionally solidified eutectic ceramic oxides. *Prog. Mater. Sci.* **2006**, *51*, 711–809. [CrossRef]
9. Pawlak, D.A.; Kolodziejak, K.; Turczynski, S.; Kisielewski, J.; Rozniatowski, K.; Diduszko, R.; Kaczkan, M.; Malinowski, M. Self-organized, rodlike, micrometer-scale microstructure of $Tb_3Sc_2Al_3O_{12}$-$TbScO_3$:Pr eutectic. *Chem. Mater.* **2006**, *18*, 2450–2457. [CrossRef]
10. Bei, H.; George, E.P. Microstructures and mechanical properties of a directionally solidified NiAl-Mo eutectic alloy. *Acta Mater.* **2005**, *53*, 69–77. [CrossRef]
11. Yanagida, T.; Fukuda, K.; Fujimoto, Y.; Kawaguchi, N.; Kurosawa, S.; Yamazaki, A.; Watanabe, K.; Futami, Y.; Yokota, Y.; Pejchal, J.; et al. Eu-doped ^{6}LiF-SrF_2 eutectic scintillators for neutron detection. *Opt. Mater.* **2012**, *34*, 868–871. [CrossRef]
12. Ohashi, Y.; Yasui, N.; Yokota, Y.; Yoshikawa, A.; Den, T. Submicron-diameter phase-separated scintillator fibers for high-resolution X-ray imaging. *App. Phy. Lett.* **2013**, *102*, 05197. [CrossRef]
13. Ohashi, Y.; Yasui, N.; Suzuki, T.; Watanabe, M.; Den, T.; Kamada, K.; Yokota, Y.; Yoshikawa, A. Orientation relationships of unidirectionally aligned $GdAlO_3/Al_2O_3$ eutectic fibers. *J. Eur. Ceram. Soc.* **2014**, *34*, 3849–3857. [CrossRef]

14. Kamada, K.; Yasui, N.; Ohashi, Y.; Den, T.; Yamaguchi, H.; Yamaji, A.; Shoji, Y.; Yoshisno, M.; Kim, K.J.; Kurosawa, S.; et al. Optimization of dopants and scintillation fibers' diameter of $GdAlO_3$/α-Al_2O_3 eutectic for high-resolution X-ray imaging. *IEEE Trans. Nucl. Sci.* **2018**, *65*, 2036–2040. [CrossRef]
15. Kamada, K.; Kurosawa, S.; Shoji, Y.; Pejchal, J.; Ohashi, Y.; Yokota, Y.; Yoshikawa, A. Luminescence and scintillation properties of Ce dope $SrHfO_3$ based eutectics. *Opt. Mater.* **2015**, *41*, 41–44. [CrossRef]
16. Kamada, K.; Kurosawa, S.; Murakami, R.; Yokota, Y.; Pejchal, J.; Ohashi, Y.; Yoshikawa, A. Growth and scintillation properties of Ce doped $Gd_2Si_2O_7$/SiO_2 eutectics. *J. Phys. Conf. Ser.* **2015**, *619*, 012036. [CrossRef]
17. Hishinuma, K.; Kamada, K.; Kurosawa, S.; Yamaji, A.; Pejchal, J.; Yokota, Y.; Ohashi, Y.; Yoshikawa, A. LiF/CaF_2/$LiBaF_3$ ternary fluoride eutectic scintillator. *Jpn. J. Appl. Phys.* **2015**, *54*, 04DH04. [CrossRef]
18. Alekhin, M.S.; de Haas, J.T.M.; Khodyuk, I.V.; Krämer, K.W.; Menge, P.R.; Ouspenski, V.; Dorenbos, P. Improvement of γ-ray energy resolution of $LaBr_3$:Ce^{3+} scintillation detectors by Sr^{2+} and Ca^{2+} co-doping. *App. Phy. Lett.* **2013**, *102*, 161915. [CrossRef]
19. Van Loef, E.V.D.; Dorenbos, P.; van Eijk, C.W.E.; Krämer, K.W.; Gudel, H.U. Scintillation properties of $LaBr_3$:Ce^{3+} crystals: Fast, efficient and high-energy-resolution scintillators. *Nucl. Instrum. Methods Phys. Res. A* **2002**, *486*, 254–258. [CrossRef]
20. Yoshikawa, A.; Epelbaum, B.M.; Hasegawa, K.; Durbin, S.D.; Fukuda, T. Microstructures in oxide eutectic fibers grown by a modified micro-pulling-down method. *J. Cryst. Growth* **1999**, *205*, 305–316. [CrossRef]
21. Jackson, K.A.; Hunt, J.D. Lamellar and rod eutectic growth. *Trans. Metall. Soc. AIME* **1966**, *236*, 1129.
22. Hunt, J.D.; Chilton, J.P. An investigation of the lamellar and rod transition in binary eutectics. *J. Inst. Met.* **1962**, *11*, 338.
23. Orera, V.M.; Pena, J.I.; Oliete, P.B.; Merino, R.I.; Larrea, A. Growth of eutectic ceramic structures by directional solidification methods. *J. Cryst. Growth* **2012**, *360*, 99–104. [CrossRef]
24. Oliete, P.B.; Mesa, M.C.; Merino, R.I.; Orera, V.M. Processing, microstructure and optical properties of the directionally solidified Al_2O_3–$EuAlO_3$ eutectic rods. *J. Cryst. Growth* **2012**, *360*, 123–126. [CrossRef]
25. Liu, S.; Lee, J.H.; Trivedi, R. Dynamic effects in the lamellar–rod eutectic transition. *Acta Mater.* **2011**, *59*, 3102–3115. [CrossRef]
26. Melcher, C.L.; Schweitzer, J.S. Cerium-doped lutetium oxyorthosilicate: A fast, efficient new scintillator. *IEEE Trans. Nucl. Sci.* **1992**, *39*, 502–505. [CrossRef]
27. Pidol, L.; Kahn-Harari, A.; Viana, B.; Virey, E.; Ferrand, B.; Dorenbos, P.; de Haas, J.T.M.; van Eijk, C.W.E. High efficiency of lutetium silicate scintillators, Ce-doped LPS, and LYSO crystals. *IEEE Trans. Nucl. Sci.* **2004**, *51*, 1084–1087. [CrossRef]